# *Silicon microring resonators tuned with GST phase change material*

Hanyu Zhang, Linjie Zhou, Jian Xu, Liangjun Lu, and Jianping Chen
*Shanghai Institute for Advanced Communication and Data Science, Shanghai Key Lab of Navigation and Location Services, State Key Laboratory of Advanced Optical Communication Systems and Networks, Department of Electronic Engineering, Shanghai Jiao Tong University*
Shanghai, China
ljzhou@sjtu.edu.cn

B. M. A. Rahman
*Department of Electrical and Electronic Engineering City, University of London*
London, U.K.
B.M.A.Rahman@city.ac.uk

***Abstract*—We investigate silicon microring resonators embedded with Ge2Sb2Te5. The phase change is induced all optically by using a sequence of optical pulses. The tuning is non-volatile and repeatable, which can be employed for optical trimming.**

***Keywords—silicon photonics, microring resonator, phase change material***

## I. INTRODUCTION

Phase change materials (PCMs) have been investigated since the 1980s for energy storage [1]. In recent years, the ability to switch rapidly and reversibly between two states with very different optical properties has found an increasingly broader variety of potential applications in photonics, including neuromorphic computing, optical memory, and photonic in-memory computing. The active tuning of silicon photonic devices is typically achieved by the thermo-optic (TO) effect [2] or the electro-optic (EO) effect [3] based on free-carrier injection, which has a refractive index tuning range in the order of 0.01 and 0.001, respectively. Thus, in order to obtain enough phase change, a relative long waveguide of 100's μm to mm length is required. The tuning also consumes significant electrical power to maintain the raised temperature in TO tuning or needs a certain free-carrier concentration in EO tuning. In a photonic integrated circuit, the device size and power consumption are becoming the bottleneck for its further scale-up in integration density. In order to reduce the power consumption, it is highly demanded to find a more efficient tuning method. The $Ge_2Sb_2Te_5$ (GST) material, as a PCM commonly used in optical storage, exhibits distinct optical (refractive index) and electrical (resistance) properties between its amorphous (*am*) and crystalline (*cr*) states [4]. Besides, its phase transition is usually reversible [5]. In addition, this material possesses the "self-holding" feature, and consequently there is no static power consumption to maintain the states [6]. Hence, it can be utilized to manipulate light propagation and implement reconfigurable non-volatile optical devices.

Here, we investigate silicon microring resonators integrated with GST material. The coupling between the microring resonator and the bus waveguide is based on a long directional coupler and thus different coupling regimes can always be attained in a small wavelength range, allowing pump and probe light to interact differently with the GST by choosing proper wavelengths.

## II. DEVICE DESIGN AND IMPLEMENTATION

Fig. 1(a) illustrates the structure of the GST-loaded silicon waveguide. The single-mode silicon waveguide height is $h$ = 220 nm and width is $w$ = 500 nm with air upper-cladding and 2-μm-thick buried oxide under-cladding. A 15-nm-thick GST layer and a 10-nm-thick indium tin oxide (ITO) layer with a length of $L_{GST}$ are placed on top of the silicon waveguide to form a hybrid waveguide. Heating the GST above the crystallization temperature (but below the melting temperature) will result in the formation of the crystalline phase. For amorphization, the GST should be heated to a temperature above the melting point and then quickly cooled to below the glass transition temperature to preserve this disordered state [7]. The phase change process of GST is reversible and repeatable, as shown in Fig. 1(b).

Fig. 1(c) illustrates the modal electric-field intensity profiles for the GST-loaded silicon waveguide in two phase states. In the amorphous phase, the optical field is mainly confined in the silicon waveguide, with an effective index of 2.51+0.00672i. In the crystalline state, on the other hand, the optical field is localized more in the GST layer, with a larger effective index of 2.69 + 0.116i. Thus, the crystalline state has a larger propagation constant and a higher optical absorption loss. The optical transmission through the GST-loaded waveguide can be efficiently modulated by changing the GST phase state.

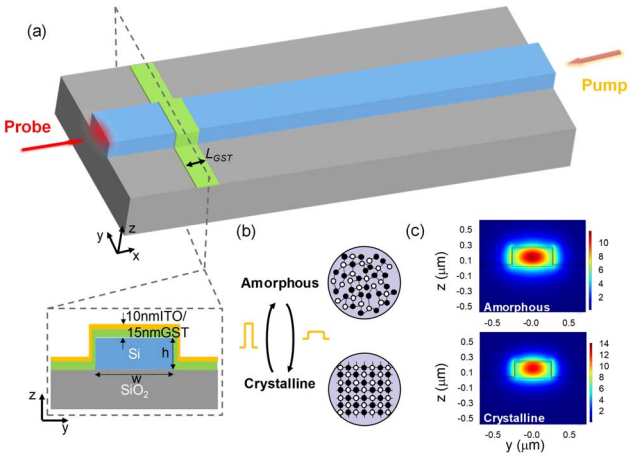


Fig. 1. (a) Schematic structure of the GST-loaded silicon waveguide. Inset shows the cross-sectional view. (b) Reversible phase change of GST material. (c) Simulated modal electric-field profiles of the Si-GST hybrid waveguide for two phase states.

The GST can also be integrated in a microring resonator to control its resonance property. Fig. 2(a) shows the structure of a microring resonator with the ring waveguide covered with a small patch of GST. The electric-field transfer function can be expressed as:

$$b_1 = \frac{-\alpha + te^{-j\theta}}{-\alpha t^* + e^{-j\theta}} a_1 \quad (1)$$

where $a_i$ and $b_i$ ($i$ = 1, 2) are the light fields before and after the microring resonator, respectively, $\alpha$ represents the optical field loss factor, $\theta$ is phase shift after one round trip in the microring resonator, and $t$ is the electric field transmission coefficient of the coupler (the coupling coefficient is $\kappa$; satisfying $|t|^2+|\kappa|^2$ for lossless coupling). The phase change of GST will modify both the real and imaginary parts of the waveguide effective refractive index, changing $\theta$ and $\alpha$ in (1), respectively. As a result, both the resonance wavelength and the extinction ratio will change accordingly.

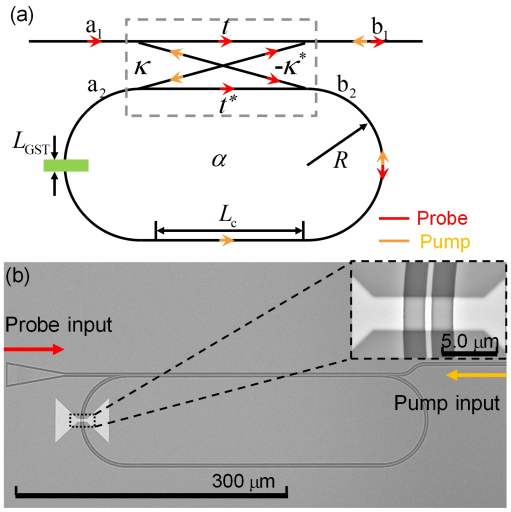


Fig. 2. (a) Microring resonator integrated with GST. (b) Scanning electron microscope image of the fabricated device. The inset shows the zoom-in of the GST-loaded ring waveguide.

## III. Device Fabrication

We fabricated the device on a silicon-on-insulator (SOI) wafer. We first used e-beam lithography (EBL) to define the silicon waveguide and microring resonator patterns. The patterns were then transferred to the silicon layer with inductively-coupled plasma (ICP) dry etch. A second EBL step was used to open the GST deposition window. GST was sputtered from a stoichiometric GST target, immediately followed by ITO sputtering deposition to protect the GST layer from oxidation. Finally, the device was placed in an acetone bath for lift-off stripping so that the GST was only left in the deposition window. Fig. 2(b) shows the scanning electron microscope (SEM) image of the microring resonator covered with a small piece of GST.

## IV. Experiment and Results

Fig. 3 depicts the counter-propagating pump & probe experimental setup to characterize the device. Pump pulses were used to change the phase of GST, while a continuous-wave (CW) probe light was used to detect the optical transmission through the device. The energy associated with the pump pulse was chosen to be high enough to heat it to its transition temperature. For the probe pulse, on the other hand, the energy was fixed to a lower level so that device spectrum could be measured without changing the GST phase state.

The pump laser was firstly modulated by an electro-optic modulator (EOM) driven by an arbitrary waveform generator (AWG) to generate optical pulses. The pulses were then amplified by an erbium-doped fiber amplifier (EDFA) followed by an optical tunable filter (OTF). Probe light and pump light were coupled to the device via apodized grating couplers from two opposite directions, and they were separated by optical circulators. The pump and probe light after the device were monitored by optical detectors.

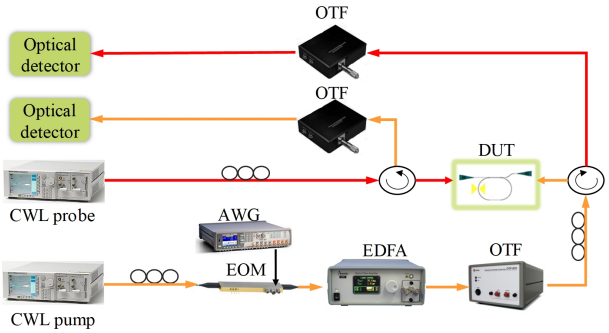


Fig. 3. Optical pump & probe experimental setup for characterizing the microring resonator.

The first microring resonator (device I) that we characterized works in the under-coupling regime in the wavelength range of 1500 to 1600 nm. The waveguide dimensions are the same with those used in the Fig. 1. The microring radius is $R$ = 50 μm. The directional coupler length is $L_c$ = 59 μm, and the gap size is 0.2 μm. The length of GST is $L_{GST}$ = 2 μm.

The crystallization of GST was induced by five identical optical pulses with a width of 50 ns (40 mW peak power) at the 1550.9 nm resonance wavelength. Each of these pulses initiated partial crystallization of the GST. Subsequently, the re-amorphization was induced by a single pulse with a width of 25 ns (56 mW peak power) at the same wavelength as the crystallization. The peak power was measured before chip coupling. The coupling loss of the grating coupler is around 5 dB/facet.

Fig. 4(a) shows the normalized spectra for two phase change cycles (two crystalline states and two amorphous states). Fig. 4(b) illustrates the magnified spectra. The amorphous state exhibits a slightly blue-shifted spectrum and a higher extinction ratio (ER). In the crystalline state, the ER is relatively small due to the high optical attenuation in the resonator. Fig. 4(c) illustrates the four intermediate states ($state_1$ to $state_4$) of the crystallization process. The amorphous phase and the crystalline phase are labeled as "off" and "on" states, respectively. We define the transmission contrast between “off” state and “on” state as their ER differences. Fig. 4(d) shows the contrast as a function of wavelength. The contrast exceeds 3 dB near the resonance wavelength. The parameters of the microring resonator can be extracted by fitting the measured spectra using (1). The extracted parameters are summarized in Table I.

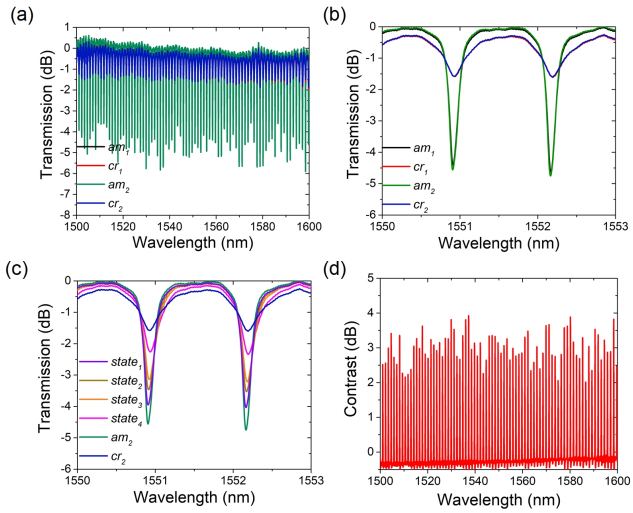


Fig. 4. (a) Measured transmission spectra of device I over two phase change cycles. (b) Magnified spectra showing two resonances. (c) Intermediate transmission spectra when the GST is partially crystallized. (d) Transmission contrast between the crystalline and amorphous states.

TABLE I. EXTRACTED MICRORING RESONATOR PARAMETERS NEAR 1550.9 NM WAVELENGTH FOR DEVICE I.

| | $am_1$ | $cr_1$ | $state_1$ | $state_2$ | $state_3$ | $state_4$ | $am_2$ | $cr_2$ |
|---|---|---|---|---|---|---|---|---|
| $\alpha$ | 0.716 | 0.392 | *0.688* | *0.652* | *0.615* | *0.501* | 0.728 | 0.390 |
| $t$ | 0.918 | 0.928 | *0.916* | *0.917* | *0.917* | *0.917* | 0.916 | 0.927 |

In the second microring resonator (device II), we further increased the coupling length so that different coupling regimes can all be observed in the 1500-1600 nm wavelength range. The coupling length is $L_c$ = 476 μm and the GST length is $L_{GST}$ = 4 μm. The other parameters are the same as device I. The crystallization was induced by three identical pulses with a width of 50 ns (31 mW peak power) at 1556.7 nm wavelength. The re-amorphization was induced by a single pulse with a width of 25 ns (56 mW peak power).

Fig. 5(a) shows the normalized spectra for two phase change cycles for device II. The insets (i), (ii) and (iii) magnify the spectra in the over-coupling, under-coupling and critical-coupling regimes, respectively. It can be seen that the transmission contrast is maximized when the resonance reaches the critical coupling point in either the amorphous or the crystalline state. Fig. 5(b) shows that, similar to device I, the resonator spectrum also exhibits intermediate states. Fig. 5(c) presents the transmission contrast between the two states, which is highly dependent on the wavelength.

In conclusion, we have investigated two silicon microring resonators integrated with a small piece of GST material on top of the ring waveguide. The phase change of GST provides a new tool to tune the resonance with "self-holding". The partial crystallization of GST by controlling the number of pump pulses also allows the presence of multiple intermediate states. This gives an effective tool to manipulate light propagation with phase change material in integrated photonic devices. These results open the way for a new class of all-optically trimmable non-volatile silicon photonic devices.

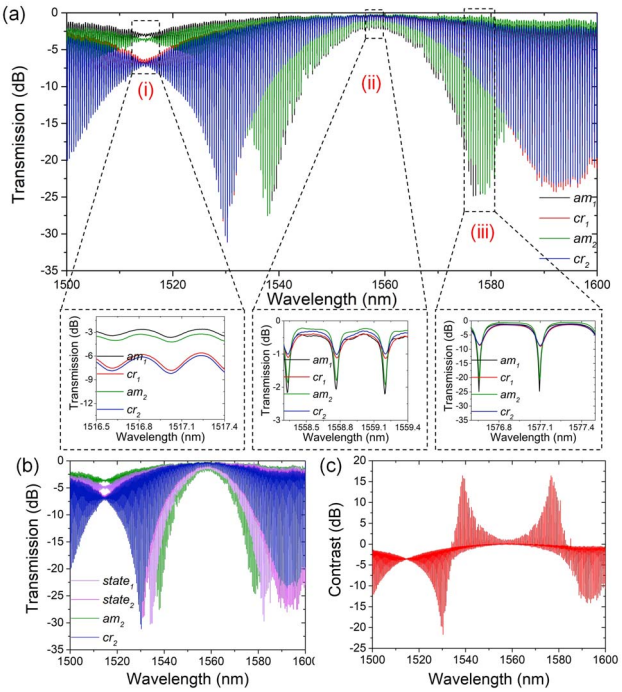


Fig. 5. (a) Measured transmission spectrum of the device II. The insets show the magnified spectra in three different coupling regimes. (b) Measured intermediate transmission spectra. (c) Transmission contrast between the crystalline and amorphous states.

TABLE II. EXTRACTED MICRORING RESONATOR PARAMETERS IN THREE COUPLING REGIMES FOR DEVICE II.

| | $\alpha_i$ | $t_i$ | $\alpha_{ii}$ | $t_{ii}$ | $\alpha_{iii}$ | $t_{iii}$ |
|---|---|---|---|---|---|---|
| $am_1$ | 0.785 | 0.119 | 0.727 | 0.970 | 0.741 | 0.739 |
| $cr_1$ | 0.548 | 0.095 | 0.478 | 0.969 | 0.514 | 0.745 |
| $am_2$ | 0.754 | 0.098 | 0.721 | 0.970 | 0.739 | 0.737 |
| $cr_2$ | 0.483 | 0.079 | 0.530 | 0.973 | 0.525 | 0.752 |

## ACKNOWLEDGMENT

This work was supported in part by the National Natural Science Foundation of China (NSFC) (61535006, 61705129, 61661130155).

## REFERENCES

[1] M. Wuttig, H. Bhaskaran, and T. Taubner, "Phase-change materials for non-volatile photonic applications," Nat. Photonics, vol. 11, pp. 465-476, 2017..

[2] L. Lu, L. Zhou, S. Li, Z. Li, X. Li, and J. Chen, "4× 4 nonblocking silicon thermo-optic switches based on multimode interferometers," J. Lightwave Technol., vol. 33, pp. 857-864, 2015

[3] L. Lu et al., "16 x 16 non-blocking silicon optical switch based on electro-optic Mach-Zehnder interferometers," Opt. Express, vol. 24, pp. 9295-307, 2016.

[4] J. Feldmann et al., "Calculating with light using a chip-scale all-optical abacus," Nat. commun., vol. 8, p. 1256, 2017.

[5] M. Rudé et al., "Optical switching at 1.55 μm in silicon racetrack resonators using phase change materials," Appl. Phys. Lett., vol. 103, p. 141119, 2013.

[6] H. Zhang et al., "Ultracompact Si-GST hybrid waveguides for nonvolatile light wave manipulation," IEEE Photonics J., vol. 10, pp. 1-10, 2018.

[7] M. Wuttig and N. Yamada, "Phase-change materials for rewriteable data storage," Nat. mater., vol. 6, pp. 824-32, 2007.